J Sol-Gel Sci Technol (2017) 84:246–257
DOI 10.1007/s10971-017-4498-5

ORIGINAL PAPER: NANO- AND MACROPOROUS MATERIALS (AEROGELS, XEROGELS, CRYOGELS, ETC.)

Synthesis of strong silica aerogel by PEDS at ambient conditions for adsorptive removal of *para*-dichlorobenzene from water

Alireza Farsad[1] · Ali Ahmadpour[1] · Tahereh Rohani Bastami[2] · Alireza Yaqubzadeh[1]

Received: 8 May 2017 / Accepted: 9 August 2017 / Published online: 7 September 2017

Abstract In this study, a strong silica aerogel was synthesized by using polyethoxydisiloxne (PEDS) as a precursor and hexamethyldisilazane (HMDZ) as a surface modifier. The obtained aerogel was characterized by scanning electron microscopy (SEM), Fourier transform infrared spectroscopy (FT-IR), and nitrogen adsorption/desorption at 77 K. The aerogel product holds a surface area of 883 m^2/g, total pore volume of 2.68 cm^3/g, and mean pore diameter of 12.14 nm. The hydrophobicity of aerogel was also investigated by contact angle of water that was measured as 140°. In order to investigate the mechanical strength of the aerogel, uniaxial compression test was performed. The result showed a compressional strength value of 44.46 MPa for the synthesized aerogel. The obtained aerogel was then used for batch adsorption experiment to remove *para*-dichlorobenzene (*p*-DCB) from water. The results showed that adsorption does not significantly correlate with the pH of solution and high adsorption capacity was obtained in the whole solution pH range of 2–10. Kinetic studies showed that the system followed pseudo-second-order model. Also, the equilibrium adsorption data was well fitted by Freundlich isotherm. Thermodynamic studies confirmed that the adsorption was spontaneous and endothermic in the studied temperature range of 299–325 K.

Graphical abstract

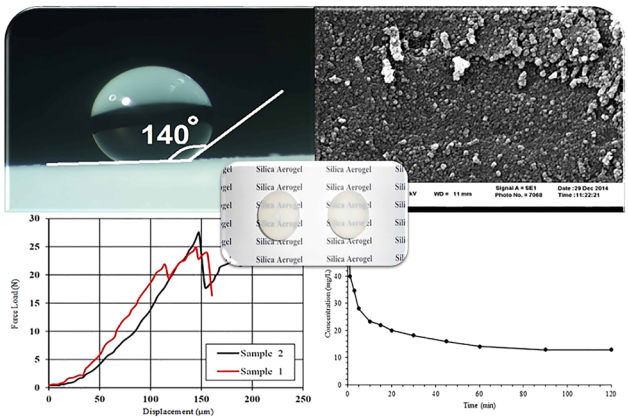

Keywords Silica aerogel · Mechanical strength · Adsorption · Kinetics · *Para*-dichlorobenzene

1 Introduction

Water treatment is an important subject because of human health and saving environment from the hazards of pollutants. Nowadays, water pollution is much more concerning than what it was before due to development of industries, agriculture, and human activities. Because of the wide range of these activities, a variety of contaminants exists in water resources, for instance biological and pharmaceutical pollutants, dyes, pesticides, heavy metals, and organic compounds. Among these types of pollutants, organic

Electronic supplementary material The online version of this article (doi:10.1007/s10971-017-4498-5) contains supplementary material, which is available to authorized users.

✉ Ali Ahmadpour
ahmadpour@um.ac.ir

[1] Department of Chemical Engineering, Faculty of Engineering, Ferdowsi University of Mashhad, Mashhad, Iran

[2] Department of Chemical Engineering, Quchan University of Advanced Technology, Quchan, Iran

contaminants are very important due to leaving hazardous effects on human health and environment. These contaminants have several types such as chlorinated compounds [1, 2], Polycyclic aromatic hydrocarbons [3], and pesticides [4]. Chlorinated aromatics are among the most hazardous and toxic contaminants threatening human and other alive species [5–7]. Some methods have been developed in order for removing these pollutions or reducing their toxicity namely membrane processing [8], biological treatment [7, 9, 10], and chemical oxidation for degradation or dechlorination [5, 9–14]. Adsorption is another important technique that is highly interested because of its ability for the removal of different kinds of contaminants such as chlorinated aromatics. Up to the time, many researches have focused on the adsorption process, by using different adsorbents, and its application toward the removal of chlorinated aromatic contaminants from aqueous solutions. For instance, one type of fungi, named Phanerochaete Chrysosporium, was used by Wu et al. [15] for biosorption of 2,4-dichlorophenol from aqueous solution with adsorption capacity of 4.09 mg/g. Activated sludge is the other adsorbent which was used for the adsorption of chlorophenol and dichlorophenol with adsorption capacity of 1.5 and 5.04 mg/g, respectively [16]. Furthermore, Graphene, a modern carbonaceous adsorbent, was used for adsorption of different polar and nonpolar toxic organic contaminants [17]. Chlorophenol and nitrophenol were also adsorbed by montmorillonite which has the adsorption capacity of 12.8 and 14.2 mg/g, respectively. Park et al. [18] modified the surface of this adsorbent via two cationic surfactants. Aksu et al. [19] used three adsorbents namely dried activated sludge, fly ash, and granular activated carbon for removal of chlorophenol isomers. Among these adsorbents, granular activated carbon revealed a better adsorption performance by removing 89.4% *p*-chlorophenol. Carbon nanotubes and activated carbon were also used for the adsorption of dichlorobenzene isomers and 4-chloronitrobenzene by Wang et al. [20]. In addition, Hernandez et al. [21] used undoped and metal-doped sol–gel substrates for adsorption of chlorobenzene as a chlorinated aromatic.

In the adsorption process, the low adsorption capacity of some adsorbents is the main issue. Some reasons for this problem are adsorbents' low surface area and porosity, their particular textural properties, or the difficulty of adsorbent synthesis process. Thus, preparation of an adsorbent with an easy synthesis procedure and good textural properties, such as high surface area and appropriate pore size distribution, provides a promising solution for the adsorption of water pollutants with high efficiency [22]. One of the most efficient adsorbents, which is used for adsorption of different organic contaminants, is aerogel [23–25]. It is currently very popular because of its unique properties. Aerogels have such a wide surface area and high porosity that help them with enhancing their performance in the adsorption process. The density of aerogels is 0.003–0.35 g/cm^3 that is much lower than water density [26]. Consequently, it can easily be separated from water after adsorption process. Another advantage is that it floats on the water surface, where most of the water pollutants accumulate; as a result, the chance of contact between aerogel and contaminants increases. Among the aerogels, those made of silica precursors have special properties, which make them proper for many applications [27–29]. Regarding its unique properties, silica aerogel is used in the present study for adsorptive removal of a chlorinated aromatic. In spite of all their advantages, conventional aerogels have a serious weakness which is their low mechanical strength and ductility that limits their performance [29, 30]. Up to the date, enhancing aerogel's mechanical strength has been the subject of many researches [27, 31–37]. Each of these studies has implemented a particular approach for enhancing aerogels mechanical properties with respect to the specific application under their consideration. Girona et al. [31] studied the effect of different factors, such as the concentration of precursor, type of solvent, and addition of fillers, on the strength of aerogels. In the best case, they obtained the compressional strength of 5.7 MPa. In another study, Parmenter et al. [32] used different fibers in the synthesis of aerogel and, as the result, an aerogel with a compressional strength of 5.37 MPa was produced. Another aerogel synthesized by Boday et al. [33] was filled with polyaniline fibers as scaffold for Si atoms. This aerogel was so ductile that could withstand under a weight of about 8500 times as its weight before facing to rupture. Sai et al. [34] also used fibers made from Acetobacter Xylinum and mixed them in the sol matrix. The resulted aerogel was very elastic with compressional strength of about 16.9 Mpa. In another study, tetraethylorthosilicate (TEOS) was mixed as the main precursor with polyhedral oligomeric silsesquioxane and led to 3.2 MPa compressional strength [27]. Although each of the mentioned approaches led to a partial increase in the compressional strength of aerogels, the most effective method in order for increasing strength is crosslinking with different polymers. Meador et al. [35] used epoxy polymer to achieve a Young's modulus of 127 MPa. In another approach, polyurea was used as the crosslinking agent and resulted in having compressional strength elevated to about 180 MPa [36]. The other polymer used for crosslinking with aerogel was polyureathane. Zhang et al. [37] implemented this polymer to obtain a flexible aerogel. Beside the interesting results of these studies, two major problems remain to be solved. The first one is the drying method [38, 39]. Most of the works performed a supercritical route to dry the gel while financially it is expensive. The other problem is the textural properties of the aerogel that become weak by enhancing its mechanical properties [35, 36, 40]. To the

best of our knowledge, there has been few aerogels synthesized with the combination of an acceptable mechanical strength and good textural properties, such as high surface area, by using drying procedure in ambient conditions.

In this research, a silica aerogel dried in ambient pressure and temperature was, first of all, synthesized while having good mechanical strength in addition to good textural properties for the adsorption process. To this sense, a prepolymerized silica precursor, called polyethoxydisiloxane (PEDS), was selected. This procedure has formerly been implemented in order for the synthesis of silica aerogel by supercritical drying method and exhibited good mechanical and textural properties [41]. In the current paper, PEDS was used for the synthesis of silica aerogel by drying at ambient pressure as a novel synthesis method. For this purpose, some of the traditional steps of the mentioned synthesis method have been improved. The resulted aerogel was then implemented for adsorptive removal of a chlorinated aromatic contaminant from water. The effect of some parameters, such as pH, adsorbent dose, time, and temperature, on the adsorption process was also studied in this paper. Isotherms, thermodynamics of adsorption, and reusability of the adsorbent were also investigated and discussed in the rest of the paper. As a model of chlorinated aromatic contaminants, 1,4-dichlorobenzene or *para*-dichlorobenzene (p-DCB) with the formula $C_6H_4Cl_2$ was used in this study. Because of the wide range of its uses, namely, as a pesticide, disinfectant and a precursor to other chemicals, it can easily accumulate in surface waters, underground waters, and wastewaters. This chemical compound is now well known as a carcinogen compound and is extremely harmful for human being [42]. Also, to the best of our knowledge, aerogel has never been used before for removal of chlorinated aromatics pollutant from water.

2 Experimental

2.1 Materials

All the materials including TEOS ($C_8H_{20}O_4Si$), ammonia (NH_4OH), ethanol (CH_3CH_2OH), sulfuric acid (H_2SO_4), hexamethyldisilazane (HMDZ) ($C_6H_{19}NSi_2$), n-hexane (C_6H_{14}), hydrochloric acid (HCl), 1,4-dichlorobenzene ($C_6H_4Cl_2$), and methanol (CH_3OH) were purchased from Merck Company and used as received with no more purification. The water used at each step of the experiments was deionized water.

2.2 Silica aerogel synthesis

TEOS, ethanol, water, and H_2SO_4 were used in the ratios presented in literature [43] for the production of PEDS-P_{750}. The production method was also copied from literature [43]. The subscript 750 comes from the formula: $c/2*1000$, where c is the molar ratio of water to TEOS and its value was chosen to be 1.5 in this study. In order to synthesize the silica aerogel, the resulted PEDS-P_{750} was mixed with ethanol in volume ratio of 7:13 for PEDS to ethanol. Gelation was started by addition of basic catalyst, here 7 M solution of NH_4OH, which was added by the amount of 2% v/v of the sol, tailoring its pH for gelation. Afterwards, as the sol became viscous, it was immediately poured into a Teflon autoclave covered with stainless steel. Gelation occurred in about 10–30 min. After having the gelation process complete, the gel was floated in ethanol followed by placing in a forced convection oven in 60 °C and aging for 24 h. During the aging time, the skeleton of aerogel becomes stronger. After 24 h, the gel was washed with ethanol and n-hexane. For surface modification and solvent exchange, a mixture of HMDZ, n-hexane, and ethanol was used in the volume ratio of 4:6:1, respectively. The role of ethanol in this procedure is important, as it lowers the rate of interaction between HMDZ and water trapped in the pores of the gel, while fast interaction would destroy the gel's structure due to its voids being collapsed. The resulted mixture was added to the gel and the autoclave was placed in the oven at 60 °C for 24 h, where solvent exchange was also occurred by n-hexane. Afterwards, it was floated in n-hexane for further solvent exchange and removal of reaction's byproducts from the structure. Then, the prepared gel was dried at ambient pressure and temperature overnight and, eventually, placed in the oven at 100 °C for completion of drying process. The product was a silica aerogel with a semi-transparent appearance and without any cracks on its structure, shown in Fig. 1.

Fig. 1 Semi-transparent and crack-free synthesized silica aerogel

2.3 Characterization of silica aerogel

To study the mechanical strength of the adsorbent, compression tests were carried out via a setup made for measurement of compression strength (home-made) [44]. The zeta potential values of the synthesized silica aerogel at different pH values were obtained to investigate the adsorbent's surface charge using a Zetaphoremetre (CAD, France). Adsorption/desorption of nitrogen at 77 K was performed on the synthesized aerogel and its isotherms were determined by a surface analyzer (BELSORP-mini II, BEL Japan Inc.) to investigate its textural properties. Prior to the analysis, the sample was out-gassed at 100 °C for 12 h to a residual pressure of 10^{-4} torr or less. Regarding the results of this test, specific surface area of the adsorbent was calculated by Brunauer–Emmett–Teller (BET) method, while the total pore volume and the pore size distribution of the aerogel were obtained by Barrett–Joyner–Halenda (BJH) method. To observe the morphology and the structure of adsorbent, a scanning electron microscopy (SEM) method was used (LEO 1450 VP). To investigate surface properties of the synthesized aerogel, Fourier transform infrared (FT-IR) was recorded between the wavenumbers 400 and 4000 cm^{-1} using Thermo Nicolet, Avatar 370 FT-IR. In addition, the contact angle of a water droplet on the aerogel's surface was measured by photographing [45] in order to investigate the hydrophobicity of synthesized adsorbent.

2.4 Batch adsorption experiments

The adsorbate in liquid-phase was *p*-DCB with molar mass of 147 g/mol and water solubility of 0.08 g/L at 25 °C. Adsorption behavior of *p*-DCB onto silica aerogel was studied through a batch procedure by using dual cells equipped with thermal jacket for fixing the operational temperature during the adsorption process. Aqueous solution of contaminant was synthesized by dissolving *p*-DCB in deionized water. To do the adsorption process, a certain amount of aerogel was transferred into the cell containing 50 mL of *p*-DCB solution with different initial known concentrations and then well stirred at the optimum time. In order to discover the inherent features of adsorption process, kinetics, mechanism and thermodynamics of the *p*-DCB adsorption onto the aerogel were studied as well as the affecting key parameters such as adsorbent dose, solution pH, time and temperature.

For investigation of adsorbent dose effect, contaminant solution with initial concentration of 60 mg/L at 28 °C was exposed to 1, 1.5, and 2 g/L of adsorbent, in separate processes. In order to study the pH effect, adsorption tests were carried out in pH range of 2–10 by contacting 1 g/L adsorbent with 60 mg/L solution of *p*-DCB at 28 °C.

Kinetics and mechanism of adsorption were investigated by conducting the adsorption process with 1 g/L adsorbent and initial *p*-DCB concentration of 60 mg/L at 26 ± 1 °C and concentration measurement in a time interval of 1–120 min. The amount of adsorbed *p*-DCB at each time per unit mass of adsorbent, q_t (mg/g), was calculated as follows:

$$q_t = \frac{(C_0 - C_t)V}{M}, \tag{1}$$

where C_0 is initial concentration while C_t represents the concentration of *p*-DCB (mg/L) at time *t*. In addition, the terms *V* and *M* denote the volume of solution (L) and the amount of adsorbent used (g), respectively.

The adsorption isotherms and thermodynamic parameters were determined at different temperatures (26, 38, and 52 °C) with different initial *p*-DCB concentrations (10–60 mg/L) at the optimum time to reach equilibrium condition. Thus, solutions with initial *p*-DCB concentrations of 10, 15, 30, 45, and 60 mg/L were contacted to 1 g/L adsorbent and adsorption process proceeded until equilibrium. The equilibrium amount of adsorbed *p*-DCB per unit mass of adsorbent, q_e (mg/g), was obtained by the following equation:

$$q_e = \frac{(C_0 - C_e)V}{M}, \tag{2}$$

where C_e is equilibrium concentration of *p*-DCB (mg/L) in the solution.

In order to study the reusability of the synthesized aerogel, regeneration of adsorbent was conducted as follows: 1 g/L of aerogel was transferred to the reactor containing 50 mL of a 60 mg/L solution of *p*-DCB at 28 °C, and was stirred for 2 h. After that, the aerogel was separated from the solution by a filter and then was placed at 50 °C for 1 h to be dried primarily. The spent aerogel was then dispersed in 10 mL methanol and was mixed for 30 min. Finally, the wet aerogel was dried again at 50 °C for 1 h. The adsorption capability of sample was then evaluated using the above procedure and this adsorption–desorption cycle was repeated for six cycles. It is notable that the spent aerogel had no shrinkage or fracture on its structure after the separation and recovery.

Concentration of *p*-DCB in the solution before and after each adsorption test was analyzed by employing a UV–Vis spectrophotometer at maximum absorbing wavelength ($\lambda =$ 222 nm). In the case of pH study, the initial pH was adjusted by HCl and NaOH solutions. The pH was measured using pH-meter (HANNA instruments, Inc.).

3 Results and discussion

3.1 Characterization of synthesized silica aerogel

To study the mechanical strength of the adsorbent, compression tests were carried out on the sample. Fracture of the sample occurred in force load of 26.15 N averagely, evidencing the value of 44.46 MPa for uniaxial compressive strength of the synthesized silica aerogel, calculated by the method mentioned in the reference [44]. This value shows a remarkable elevation in mechanical strength of synthesized aerogel in comparison with the conventional silica aerogels [46]. Table 1 represents the parameters obtained from the mechanical test and Fig. 2 illustrates the force load vs. diameter displacement for two discrete aerogels. Compared to the other studies aiming at the increase of aerogel's mechanical strength, except those with crosslinking method used, the present work shows a noticeably higher mechanical strength [31, 32, 34]. By implementing the crosslinking method, strong polymeric chains fill the structure of aerogel that leads to a more robust network, although it destroys the aerogel's textural properties. The increase of strength in this study was achieved by just changing the precursor and synthesis procedure. Thus, the strength value obtained here is substantially lower than the values acquired from crosslinking method. However, textural properties should be comprised to the other methods for further investigation and optimization for adsorption process.

The SEM micrographs of synthesized silica aerogel is shown in Fig. 3 in two different magnifications. It is clear that silica network of the aerogel is formed properly and the aggregations of the secondary particles can obviously be seen. As shown in the micrograph image, the aerogel's network consists of many bulks. These bulks are formed by aggregation of secondary particles which are comprised of smaller primary particles [37]. The largest evident particles in the present micrograph are these bulks. In according to the graph, the bulks' size can be estimated about 100 nm or even smaller. Consequently, as evidently seen in Fig. 3b, the size of secondary particles would be about 10 nm which is the normal size in silica aerogels [37].

The density of prepared aerogel was determined about 0.32 g/cm^3 by using helium pycnometry. Although this value is more than the density of conventional aerogels dried by supercritical method, it is in the range of aerogels' density [26].

Table 1 Data of uniaxial compression test on the synthesized silica aerogel

Sample	Sample shape	Diameter (mm)	Force load (N)	Compression strength (MPa)
1	Spherical	3	24.85	42.21
2	Spherical	3	27.45	46.72

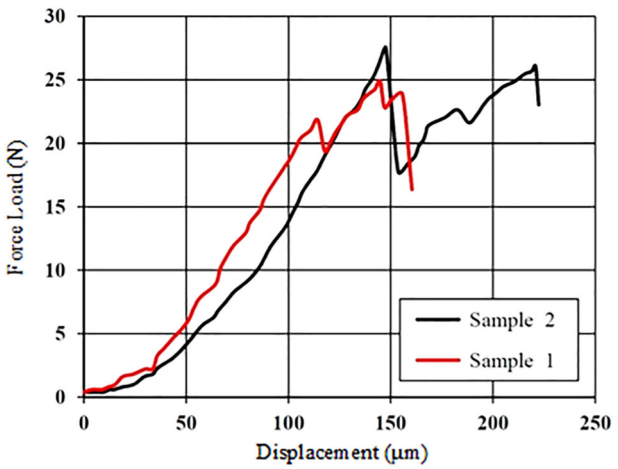

Fig. 2 Plot of uniaxial compression test on two spherical aerogels with 3 mm diameter

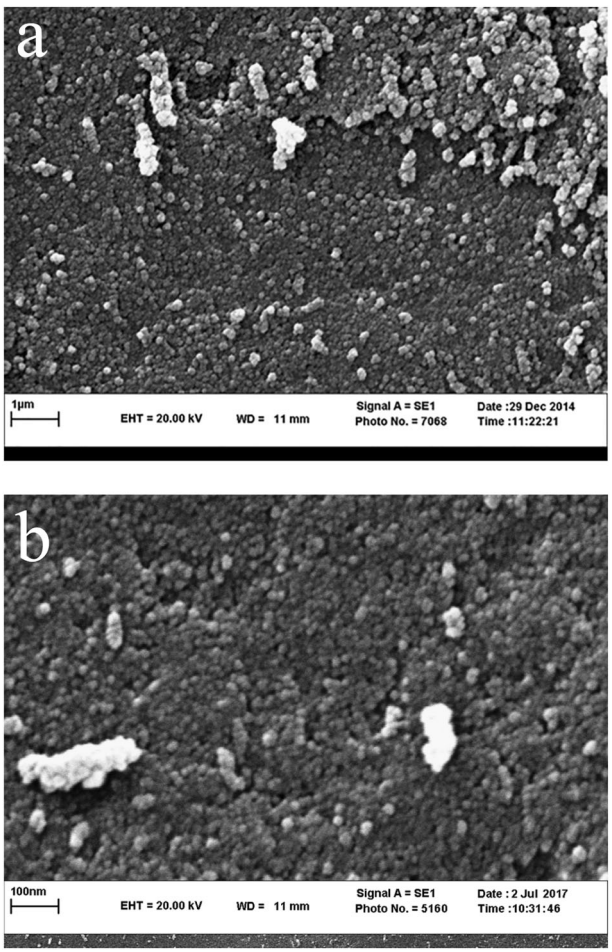

Fig. 3 Scanning electron micrographs of synthesized silica aerogel (**a** magnification of 1 μm, **b** magnification of 100 nm)

Figure 4 shows a photograph of a water droplet on the surface of synthesized aerogel. It is concluded from the figure that the contact angle between the droplet and surface of the aerogel is about 140° which shows good hydrophobicity of the prepared aerogel. This observation confirms that the surface modification of the aerogel was successfully done by HMDZ. It is suggested that the methyl group of HMDZ led to the surface hydrophobicity.

Figure 5 illustrates the FTIR spectrum of synthesized silica aerogel to study the surface of aerogel. The peaks at 467, 800, and 1096 cm^{-1} assigned to Si–O–Si bonds which confirm excellent formation of silica network in the structure of the synthesized silica aerogel [47]. As expected, the $–CH_3$ vibrations at 855 and 2970 cm^{-1} are present in the synthesized aerogel which are the result of successful surface modification by HMDZ, leading to proper hydrophobicity of silica aerogel.

The peaks at 3444 and 959 cm^{-1} could be assigned to –OH and Si–OH vibrations, respectively, which are weak due to the reaction of methyl group of HMDZ with –OH groups leading to the replacement of $O–Si(CH_3)_3$ with –OH groups. This result confirms the hydrophobicity of the prepared aerogel.

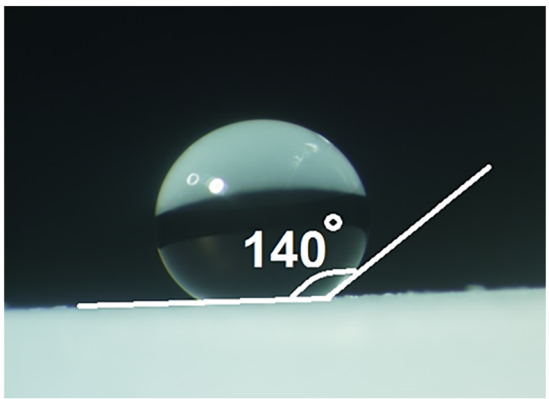

Fig. 4 Contact angle of water droplet on aerogel's surface

Figure S1 shows the isotherm of nitrogen adsorption/desorption and pore size distribution of the adsorbent. As seen in this figure, a hysteresis occurs on the desorption branch which is the result of capillary condensation in mesopores. In according to International Union of Pure and Applied Chemistry (IUPAC) theory, this type of hysteresis is related to the porous materials with complex structure containing both types of micropores and mesopores [48]. Figure S1-b clears that the most of the pores have a diameter between 1 and 20 nm. These values are in the range of micropores and mesopores. The highest peak is also related to the size of 2.71 nm. Mean pore diameter obtained from BET method is 12.14 nm which is in mesopore range, while total pore volume of the adsorbent is obtained as 2.68 cm^3/g which can provide numerous number of adsorption sites and responsible volume. Also, the specific surface area obtained from BET method is 883 m^2/g which is higher compared to most of the other aerogels with enhanced mechanical strength [27, 31, 32, 34–36].

The method used in this research for the synthesis of silica aerogel led to an aerogel with a proper mechanical strength, while its textural properties were not ruined. This approach becomes more outstanding regarding the great economic and easy drying method which has been done at ambient pressure.

3.2 Adsorption experiments

3.2.1 Effect of pH

The effect of initial pH was studied on the adsorption of *p*-DCB onto synthesized aerogel. To evaluate the effect of pH

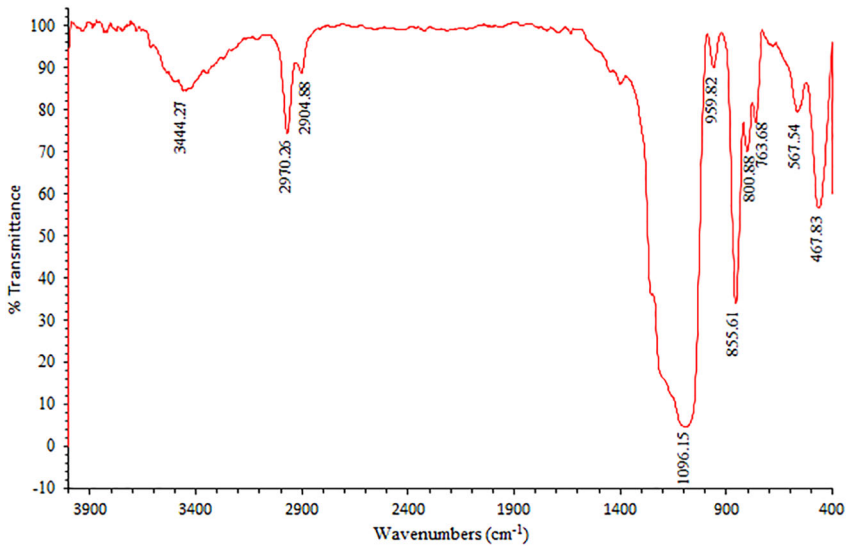

Fig. 5 FT-IR analysis of synthesized silica aerogel showing its surface functional groups

on the *p*-DCB sorption in 120 min, different experiments were conducted at 26 ± s1 °C in the pH range of 2–10 using 0.05 g of synthesized aerogel with 50 mL of 60 mg/L adsorbate solution. Figure 6 shows the adsorbed amount of *p*-DCB onto the synthesized silica aerogel in different pH values. As clearly shown in the figure, the amount of *p*-DCB adsorption tends to change negligibly with change of initial pH. In addition, the synthesized silica aerogel was able to significantly adsorb contaminant molecules at a wide pH range of 2–10. It is suggested that pH of solution has not significantly affect the surface properties of synthesized aerogel and also the molecular structure of *p*-DCB. Figure 7 illustrates the data for Zeta potential of synthesized adsorbent surface as the function of pH value. It is obviously seen that the aerogel's surface charge is close to zero in all pH ranges confirming that pH value does not have a significant effect on the adsorbent surface. On the other hand, *p*-DCB molecule does not have any acidic/basic proton and, thus, no pK_a value is available for this component. As a result, pH value does not have any significant effect on the molecular structure of *p*-DCB. Furthermore, as the log $K_{oct/wat}$ value of *p*-DCB is 3.37, its molecules can easily attend in hydrophobic media [49], the surface of synthesized silica aerogel in our case. Consequently, the adsorption properties of *p*-DCB onto surface of synthesized silica aerogel do not depend on pH of medium.

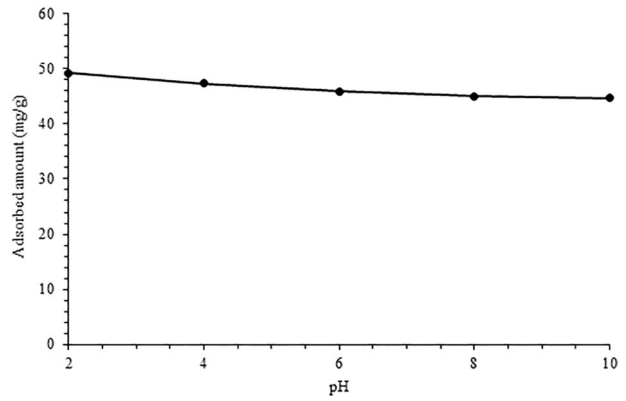

Fig. 6 Effect of pH on the adsorption of p-DCB onto silica aerogel (initial concentration = 60 mg/L, $T = 28 \pm 1$ °C, adsorbent dose = 1 g/L)

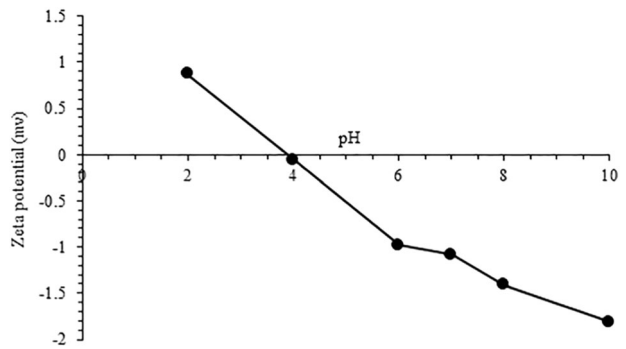

Fig. 7 Zeta potential data as a function of pH value for synthesized silica aerogel

3.2.2 Effect of mass of sorbent

Figure 8 shows removal percentage of *p*-DCB from its aqueous solution with initial concentration of 60 mg/L by 1, 1.5, and 2 g/L of adsorbent at pH = 4 and temperature of 26 ± 1 °C. The removal percentage was calculated as:

$$\text{The percent of removal} = \frac{C_0 - C_e}{C_0} \times 100, \quad (3)$$

where C_0 (mg/L) is initial concentration and C_e (mg/L) is concentration at equilibrium. It was observed in the figure that with increase in adsorbent dose, the removal percentage was elevated. This is because of the increase in active available adsorption sites of the adsorbent which enhances the interaction between adsorbate and adsorbent [50].

3.2.3 Effect of contact time and kinetic study

Figure 9 shows the effect of contact time on the removal of *p*-DCB mass of 1 g/L over a time of 1–120 min by using 60 mg/L *p*-DCB at pH = 4 and temperature 26 ± 1 °C. The removal efficiency was about 75% during 5 min. The rapid increase of removal efficiency in the initial stages indicated that there were plenty of readily accessible sites due to high specific surface area and proper pore size and volume of the synthesized aerogel. By moving forward through the time, the concentration of adsorbate in solution becomes decreases, while its concentration in adsorbent voids elevates continuously. Thus, the driving force for the adsorption process reduces which leads to reduction of adsorption efficiency in longer time [51, 52]. This is why the slope of the plot decreases with increase of time. Equilibrium seems

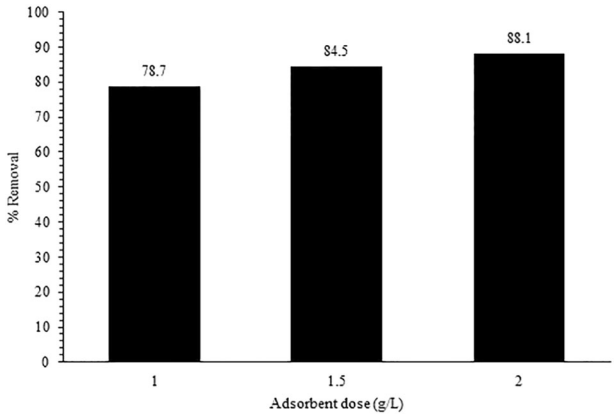

Fig. 8 Effect of mass of adsorbent for the removal of p-DCB onto silica aerogel (initial concentration= 60 mg/L, $T = 28 \pm 1$ °C, pH = 4)

to occur after 90 min; however, the adsorption process was continued up to 120 min in order to be confidence about reaching equilibrium state.

To study adsorption kinetic, pseudo-first-order (Eq. 4), and pseudo-second-order (Eq. 5) models were applied as following [53–55]:

$$\log(q_e - q_t) = \log q_e - \frac{K_1 t}{2.303}, \quad (4)$$

$$\frac{t}{q_t} = \frac{1}{K_2 q_e^2} + \frac{t}{q_e}, \quad (5)$$

where K_1 and K_2 are pseudo-first-order and pseudo-second-order coefficients which units are time^{-1} and g/mg time, respectively. The curves of pseudo-first-order and pseudo-second-order models, correlated to the experimental data of *p*-DCB adsorption by silica aerogel are shown in Fig. S2. In addition, the rate constants, correlation coefficients, and the experimental and calculated uptake capacity (q_e, mg/g) are presented in Table 2. It was found that pseudo-second-order has more correspondence with obtained data. Correlation coefficient of determination (R^2) is 0.999 for this model. Divergence between the amount of q_e predicted by this model and what obtained from experiments is less than the case of pseudo-first-order model which is another proof for compatibility of pseudo-second-order model for this adsorption system. This model corresponds to systems with chemical adsorption. Thus, the process of *p*-DCB adsorption by synthesized silica aerogel is also chemical.

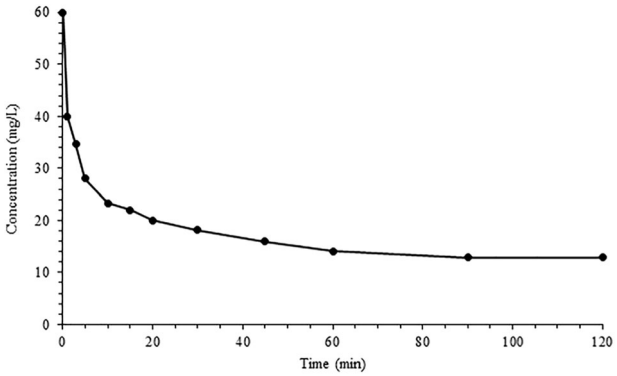

Fig. 9 Effect of contact time on the adsorption of p-DCB onto silica aerogel (initial concentration = 60 mg/L, $T = 28 \pm 1$ °C, adsorbent dose = 1 g/L)

In order to investigate the mechanism of adsorption, inter-particle diffusion model was applied [56, 57] as:

$$q_t = K_{int} t^{0.5} + C, \quad (6)$$

where K_{int} (mg/g time$^{0.5}$) denotes inter-particle diffusion coefficient and term C (mg/g) is a constant parameter related to boundary layer thickness. Figure 10 presents the plot of this model fitted with experimental data of this study. It is obvious in Fig. 10 that this adsorption process has three steps. The first step is adsorption on the adsorbent surface which is very fast and occurs in a short time. The second one is related to diffusion and adsorption on inter-particle voids which has more moderate slope compared to the first step. The final step represents the equilibrium of adsorption which has a very small slope. The model coefficients obtained from inter-particle diffusion theory are presented in Table 3. The term C has increase at each step that shows the increase of boundary layer thickness. In addition, it is shown in Table 3 that the term K, the ability of adsorption and diffusion, reduces by time.

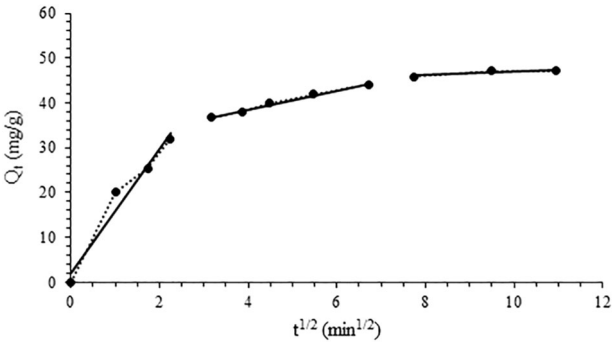

Fig. 10 Plot of interparticle diffusion model correlated to the experimental adsorption data of p-DCB by silica aerogel (initial concentration = 60 mg/L, $T = 28$ °C, adsorbent dose = 1 g/L)

Table 3 Parameters of interparticle diffusion model for adsorption of *p*-DCB on silica aerogel

	First step	Second step	Third step
K_{int} (mg/g min)	13.9	2.1	0.4
C (mg/g)	2.1	30.1	42.9

Table 2 Parameters of kinetics models obtained for adsorption of *p*-DCB by silica aerogel (initial conc. = 60 mg/L, $T = 26 \pm 1$ °C, adsorbent dose=1 g/L)

Pseudo-first-order model				Pseudo-second-order model			
R^2	K_1 (min^{-1})	q_e (cal.) (mg/g)	q_e (exp.) (mg/g)	R^2	K_2 (g/mg min)	q_e (cal.) (mg/g)	q_e (exp) (mg/g)
0.921	0.05	24.8	47.2	0.999	0.006	48.3	47.2

3.2.4 Adsorption isotherm model

The results were analyzed with the well-known models of Langmuir and Freundlich isotherms [54, 58, 59] which are described by following equations:

$$q_e = \frac{q_{\mathrm{ml}} K_l C_{\mathrm{e}}}{1 + K_l C_{\mathrm{e}}}, \tag{7}$$

$$q_{\mathrm{e}} = K_{\mathrm{f}} C_{\mathrm{e}}^{1/n}, \tag{8}$$

where q_{m} is monolayer adsorption capacity (mg/g), K_{l} is Langmuir constant (L/mg), and the terms K_{f} ((mg/g)(L/mg)$^{1/n}$) and n are Freundlich constants. In order to investigate the isotherms, linear form of Langmuir isotherm and logarithmic form of Freundlich isotherm should be used as:

$$\frac{C_{\mathrm{e}}}{q_{\mathrm{e}}} = \frac{1}{q_{\mathrm{ml}} K_l} + C_{\mathrm{e}}\left(\frac{1}{q_{\mathrm{ml}}}\right), \tag{9}$$

$$\log q_{\mathrm{e}} = \frac{1}{n} \log C_{\mathrm{e}} + \log K_{\mathrm{f}}. \tag{10}$$

Figure S3 illustrates the changes of *p*-DCB adsorption by silica aerogel for the isotherms under study and their agreement with experimental data. Table 4 also presents the values of isotherms' parameters obtained from above equations. It is shown in the table that this adsorption system is a better fit to Freundlich isotherm rather than Langmuir isotherm. The R^2 value is over 0.999 for Freundlich isotherm. This isotherm is responsible for systems with multilayer adsorption, while the active sites of their adsorbent are heterogeneous [60]. These heterogeneities can be the result of surface modification by HMDZ and settlement of CH_3 species on the aerogel surface. In fact, adsorption of *p*-DCB can be done by CH_3 functional groups. The value of the term n in Freundlich isotherm is very important such that it stands for a good adsorption system if it takes a value between 1 and 10. For the system presented in this paper, n is calculated equal to 1.51 that shows an appropriate adsorption, while its near unity value indicates that the surface of adsorbent is homogeneous. This fact is proved with respect to the R^2 value obtained from Langmuir isotherm which is not too far from 1.

Table 4 Isotherm parameters for adsorption data of *p*-DCB by silica aerogel

Freundlich			Langmuir		
R^2	n	K_{f} ((mg/g)(L/mg)$^{1/n}$)	R^2	K_{l} (L/mg)	q_{m} (mg/g)
0.999	1.51	8.79	0.963	0.111	77.52

3.2.5 Thermodynamic parameters of sorption

In order to study the mechanism of sorption process of *p*-DCB onto synthesized aerogel, thermodynamic parameters such as change in Gibbs free energy (ΔG°), enthalpy (ΔH°), and entropy (ΔS°) were investigated. These parameters are calculated using following equations [54, 61]:

$$K_{\mathrm{c}} = \frac{C_{\mathrm{a}}}{C_{\mathrm{e}}}, \tag{11}$$

$$\Delta G^\circ = -RT \ln K_c \tag{12}$$

$$\Delta G^\circ = \Delta H^\circ - T\Delta S^\circ, \tag{13}$$

where K_{c} is distribution coefficient of adsorption, C_{a} is equilibrium concentration of *p*-DCB in aerogel's pores (mg/L), the term R is universal gas law constant that takes the value of 8.314 J/mol K, and T is absolute temperature (K). Change in Gibbs free energy is directly calculated from Eq. 12. By plotting ΔG° vs. T, the change in enthalpy and entropy are evaluated from the intercept and slope of the plot, respectively. Table 5 represents the obtained thermodynamic parameters of this adsorption system. The negative values of ΔG° at all temperatures indicate the feasibility of the process and confirm spontaneity of adsorption, which elevates with increase in temperature [54, 61]. The value of ΔH° is positive which indicates that the adsorption process is endothermic [61]. The value of ΔS° is also positive that confirms increase in the randomness of the adsorbent and solution interface during the adsorption process [61].

3.2.6 Regeneration study

One of the most important principles in adsorption systems, especially in pilot or industrial scale, is economic factor. The removal efficiency of the synthesized aerogel during adsorption/desorption cycles are shown in Fig. 11. It can be observed that the adsorption capacity remains constant only after first cycle. Furthermore, it is obvious that after each cycle, the structure of adsorbent is not destroyed and adsorption process is performed as successfully as the first time with a little divergence. Figure 12 shows the SEM image of spent aerogel after six sequential adsorption/desorption cycles. It is clear that the structure of aerogel is not destroyed during regeneration process. This is one of the

Table 5 Thermodynamic parameters of *p*-DCB adsorption by silica aerogel (adsorbent dose = 1 mg/L)

T (K)	ΔG° (KJ/mol)	ΔH° (KJ/mol)	ΔS° (KJ/mol)
299	−26.5		
311	−34.8	112.9	0.47
325	−38.9		

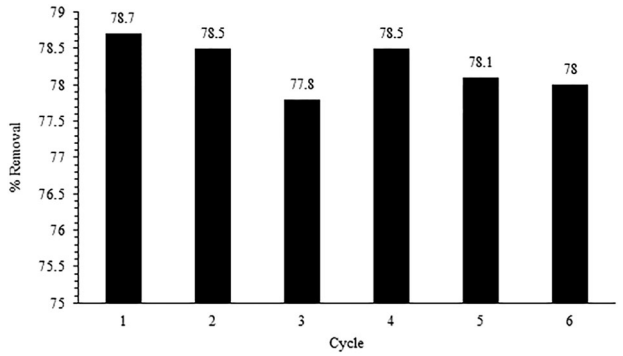

Fig. 11 Removal percent of p-DCB from water by silica aerogel after each regeneration cycle (initial concentration = 60 mg/L, $T = 28$ °C, adsorbent dose = 1 g/L)

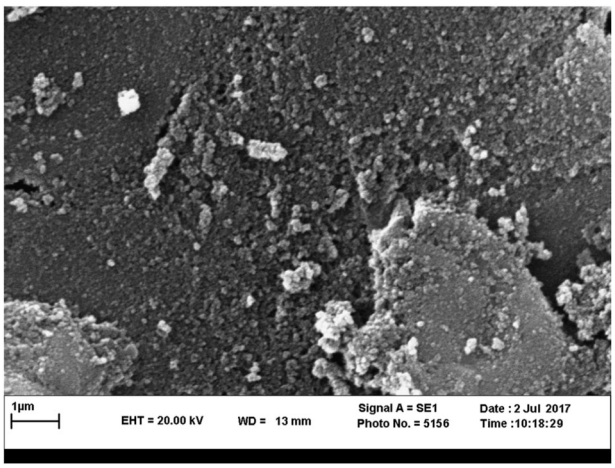

Fig. 12 SEM image of spent silica aerogel after six cycles of adsorption/desorption process

important and valuable characteristics of the synthesized silica aerogel that proves its economical advantage and verifies that it may widely been used for industrial purposes.

4 Conclusion

In this research, PEDS-P_{750} was used for synthesis of a strong silica aerogel. Surface modification was performed by HMDZ and drying process was at ambient temperature and pressure. Compression test on the synthesized aerogel confirmed enhancement of its mechanical strength. Proper formation of the aerogel's silica network was observed by SEM image. By using FT-IR analysis, functional groups on the aerogel's surface, such as Si–O–Si, –OH, Si–OH, and $-CH_3$ vibrations, were investigated to study the aerogel's surface. Complete formation of silica structure, reduction of hydrophilicity, and settlement of hydrophobic CH_3 groups were obviously seen that proves the success of surface modification reaction by HMDZ. Hydrophobicity of the synthesized aerogel was also investigated by measuring the contact angle between the water droplet and the adsorbent's surface which was high. In addition, nitrogen adsorption/desorption at 77 K confirmed excellent textural properties of synthesized aerogel including high specific surface area and proper pore volume and pore size distribution.

The synthesized silica aerogel was used for removal of *p*-DCB from water media by batch adsorption tests and the effects of different key parameters such as temperature, pH, adsorbent dose, initial contaminant solution concentration, and time on the adsorption process were studied. Our results show that increase of adsorbent leads to more removal efficiency of contaminant and the adsorbed amount of *p*-DCB does not change significantly with change of solution pH. It was observed from kinetic studies that the kinetic of adsorption obeys the pseudo-second-order model that is implemented to chemical adsorption processes. The mechanism of adsorption was investigated by inter-particle diffusion theory and included three steps: quick surface adsorption, diffusion and adsorption in voids, and equilibrium of adsorption process. Isotherm study confirmed that Freundlich isotherm is a good fit to adsorption equilibrium data rather than Langmuir isotherm. Thermodynamic study also confirmed that the adsorption is spontaneous (especially at higher temperatures), endothermic, and is accompanied with increase of randomness in adsorbent/solution interface. Finally, regeneration of adsorbent was carried out for six cycles and the results shows that this aerogel is economical and reusable.

The acceptable high mechanical strength of this silica aerogel, its good textural properties, and drying process, which was done at ambient pressure, all together, have made this synthesized aerogel unique. All of the investigations done in this research proved that this strong silica aerogel can be used for removal of *p*-DCB (and probably other types of nonpolar organic contaminants, especially chlorinated aromatics) from water.

Compliance with ethical standards

Conflict of interest The authors declare that they have no competing interests.

References

1. Baric M, Majone M, Beccari M, Papini MP (2012) Coupling of polyhydroxybutyrate (PHB) and zero valent iron (ZVI) for enhanced treatment of chlorinated ethanes in permeable reactive barriers (PRBs). Chem Eng J 195–196:22–30
2. Lemus J, Martin-Martinez M, Palomar J, Gomez-Sainero L, Gilarranz MA, Rodriguez JJ (2012) Removal of chlorinated

organic volatile compounds by gas phase adsorption with activated carbon. Chem Eng J 211–212:246–254
3. Rauscher L, Sakulthaew C, Comfort S (2012) Using slow-release permanganate candles to remediate PAH-contaminated water. J Hazard Mater 241-242:441–449
4. Finizio A, Azimonti G, Villa S (2011) Occurrence of pesticides in surface water bodies: a critical analysis of the Italian national pesticide survey programs. J Environ Monit 13:49–57
5. Yang J, Gao Y, Xu D, Cao L, Jia J (2012) A controllable Fe^0–C permeable reactive barrier for 1,4-dichlorobenzene dechlorination. Chem Eng J 203:166–173
6. Linnie MJ, Keatinge MJ (2000) Pest control in museums: toxicity of para-dichlorobenzene, 'Vapona', and naphthalene against all stages in the life-cycle of museum pests, dermestes maculatus degeer, and anthrenus verbasci (L.) (Coleoptera: Dermestidae). Int Biodeterior Biodegrad 45:1–13
7. Hoskeri RS, Mulla SI, Ninnekar HZ (2014) Biodegradation of chloroaromatic pollutants by bacterial consortium immobilized in polyurethene foam and other matrices. Biocatal Agric Biotechnol 3:390–396
8. Rodriguez C, Linge K, Blair P, Busetti F, Devine B, Van Buynder P, Weinstein P, Cook A (2012) Recycled water: Potential health risks from volatile organic compounds and use of 1,4-dichlorobenzene as treatment performance indicator. Water Res 46:93–106
9. Topping B (1987) The biodegeradability of *para*-dichlorobeenzene and its behavior in model activated sludge plants. Water Res 21:295–300
10. Lee SH, Lee SH, Ryu SJ, Kang CS, Suma Y, Kim HS (2013) Effective biochemical decomposition of chlorinated aromatic hydrocarbons with a biocatalyst immobilized on a natural enzyme support. Bioresour Technol 141:89–96
11. Lichtenberger J, Amiridis MD (2004) Catalytic oxidation of chlorinated benzenes over V_2O_5/TiO_2 catalysts. J Catal 223:296–308
12. Jin L, Shah YT, Abraham MA (1990) The effect of supercritical water on the catalytic oxidation of 1,4-dichlorobenzene. J Supercrit Fluids 3:233–239
13. Fu F, Dionysiou DD, Liu H (2014) The use of zero-valent iron for groundwater remediation and wastewater treatment: a review. J Hazard Mater 267:194–205
14. Selli E, Bianchi CL, Pirola C, Cappelletti G, Ragaini V (2008) Efficiency of 1,4-dichlorobenzene degradation in water under photolysis, photocatalysis on TiO_2 and sonolysis. J Hazard Mater 153:1136–1141
15. Wu J, Yu HQ (2006) Biosorption of 2,4-dichlorophenol from aqueous solution by Phanerochaete chrysosporium biomass: isotherms, kinetics and thermodynamics. J Hazard Mater B 137:498–508
16. Ruiying G, Wang J (2007) Effects of pH and temperature on isotherm parameters of chlorophenols biosorption to anaerobic granular sludge. J Hazard Mater 145:398–403
17. Chowdhury S, Balasubramanian R (2014) Recent advances in the use of graphene-family nanoadsorbents for removal of toxic pollutants from wastewater. Adv Colloid Interface Sci 204:35–56
18. Park Y, Ayoko GA, Kurdi R, Horváth E, Kristóf J, Frost RL (2013) Adsorption of phenolic compounds by organoclays: implications for the removal of organic pollutants from aqueous media. J Colloid Interface Sci 406:196–208
19. Aksu Z, Yener J (2001) A comparative adsorption/biosorption study of mono-chlorinated phenols ontp various sorbents. Waste Manage 21:695–702
20. Wang B, Chen W, Fu H, Qu X, Zheng S, Xu Z, Zhu D (2014) Comparison of adsorption isotherms of single-ringed compounds between carbon nanomaterials and porous carbonaceous materials over six-order-of-magnitude concentration range. Carbon N Y 79:203–212
21. Hernandez MA, Gonzalez AI, Corona L, Hernandez F, Rojas F, Asomoza M, Solıs S, Portillo R, Salgado MA (2009) Chlorobenzene, chloroform, and carbon tetrachloride adsorption on undoped and metal-doped sol–gel substrates (SiO_2, Ag/SiO_2, Cu/SiO_2 and Fe/SiO_2). J Hazard Mater 162:254–263
22. Rizzo L, Fiorentino A, Grassi M, Attanasio D, Guida M (2015) Advanced treatment of urban wastewater by sand filtration and graphene adsorption for wastewater reuse: effect on a mixture of pharmaceuticals and toxicity. J Environ Chem Eng 3:122–128
23. Matias T, Marques J, Quina MJ, Gando-Ferreira L, Valente AJM, Portugal A, Durães L (2015) Silica-based aerogels as adsorbents for phenol-derivative compounds. Colloid Surf A 480:260–269
24. Wang D, McLaughlin E, Pfeffer R, Lin YS (2012) Adsorption of oils from pure liquid and oil–water emulsion on hydrophobic silica aerogels. Sep Purif Technol 99:28–35
25. Mohammadi A, Moghaddas J (2014) Synthesis adsorption and regeneration of nanoporous silica aerogel and silica aerogel-activated carbon composites. Chem Eng Res Des 94:475–484
26. Kocon L, Despetis F, Phalippou J (1998) Ultralow density silica aerogels by alcohol supercritical drying. J Non-Cryst Solids 225:96–100
27. Duan Y, Jana SC, Reinsel AM, Lama B, Espe MP (2012) Surface modification and reinforcement of silica aerogels using polyhedral oligomeric silsesquioxanes. Langmuir 28:15362–15371
28. Gurav JL, Jung I, Park H, Kang ES, Nadargi DY (2010) Silica aerogel: synthesis and applications, J Nanomater 2010:1–12
29. Obrey KAD, Wilson KV, Loy DA (2011) Enhancing mechanical properties of silica aerogels. J Non-Cryst Solids 357:3435–3441
30. Capadona LA, Meador MAB, Alunni A, Fabrizio EF, Vassilaras P, Leventis N (2006) Flexible, low-density polymer crosslinked silica aerogels. Polymer 47:5754–5761
31. Girona MM, Martinez E, Roig A, Esteve J, Molins E (2001) Mechanical properties of silica aerogels measured by microindentation: influence of sol–gel processing parameters and carbon addition. J Non-Cryst Solids 285:244–250
32. Parmenter KE, Milstein F (1998) Mechanical properties of silica aerogels. J Non-Cryst Solids 223:179–189
33. Boday DJ, Muriithi B, Stover RJ, Loy DA (2012) Polyaniline nanofiber–silica composite aerogels. J Non-Cryst Solids 358:1575–1580
34. Sai H, Xing L, Xiang J, Cui L, Jiao J, Jao C, Li Z, Li F (2013) Flexible aerogels based on an interpenetrating network of bacterial cellulose and silica by a non-supercritical drying process. J Mater Chem A 1:7963–7970
35. Meador MAB, Ilhan F, Dass A, Zhang G, Vassilaras P, Johnston JC, Leventis N (2005) Crosslinking amine-modified silica aerogels with epoxies: mechanically strong lightweight materials. Chem Mater 17:1085–1098
36. Leventis N, Leventis CS, Zhang G, Ravashdeh AMM (2002) Nanoengineering strong silica aerogels. Nano Lett 2:957–960
37. Zhang G, Dass A, Rawashdeh AMM, Thomas J, Counsil JA, Leventis CS, Fabrizio EF, Ilhan F, Vassilaras P, Scheiman DA, McCorkle L, Palczer A, Johnston JC, Meador MA, Leventis N (2004) Isocyanate-crosslinked silica aerogel monoliths: preparation and characterization. J Non-Cryst Solids 350:152–164
38. Dourbash A, Motahari S, Omranpour H (2014) Effect of water content on properties of one-step catalyzed silica aerogels via ambient pressure drying. J Non-Cryst Solids 405:135–140
39. Shao Z, Wu G, Cheng X, Zhang Y (2012) Rapid synthesis of amine cross-linked epoxy and methyl co-modified silica aerogels by ambient pressure drying. J Non-Cryst Solids 358:2612–2615
40. Meador MAB, Vivod SL, McCorkle L, Quade D, Sullivan RM, Ghosn LJ, Clark N, Capadona LA (2008) Reinforcing polymer

cross-linked aerogels with carbon nanofibers. J Mater Chem 18:1843–1852
41. Wong JCH, Kaymak H, Brunner S, Koebel M (2014) Mechanical properties of monolithic silica aerogels made from polyethoxydisiloxanes. Microporous Mesoporous Mater 183:23–29
42. Butterworth BE, Ailward LL, Hays SM (2007) A mechanism-based cancer risk assessment for 1,4-dichlorobenzene. Regul Toxicol Pharm 49:138–148
43. Deng Z, Wang J, Wei J, Shen J, Zhou B, Chen L (2000) Physical properties of silica aerogels prepared with polyethoxydisiloxane. J Sol–Gel Sci Technol 19:677–680
44. Cheshomi A, Ahmadi Sheshde E (2013) Determination of uniaxial compressive strength of microcrystalline limestone using single particles load test. J Petrol Sci Eng 111:121–126
45. Liu H, Sha W, Cooper AT, Fan M (2009) Preparation and characterization of a novel silica aerogel as adsorbent for toxic organic compounds. Colloid Surf A 347:38–44
46. Ma HS, Roberts AP, Pre´vost JH, Jullien R, Scherer GW (2000) Mechanical structure–property relationship of aerogels. J Non-Cryst Solids 277:127–141
47. Shi F, Wang LJ, Liu JX (2006) Synthesis and characterization of silica aerogels by a novel fast ambient pressure drying process. Mater Lett 60:3718–3722
48. Thommes M (2010) Physical adsorption characterization of nanoporous materials. Chemie Ingenieur Technik 82:1059–1073
49. Kong XQ, Shea D, Baynes RE, Riviere JE, Xia XR (2007) Regression method of the hydrophobicity ruler approach for determining octanol/water partition coefficients of very hydrophobic compounds. Chemosphere 66:1086–1093
50. Nasuha N, Hameed BH, Mohd Din AT (2010) Rejected tea as a potential low-cost adsorbent for the removal of methylene blue. J Hazard Mater 175:126–132
51. Tsai WT, Chen HR (2010) Removal of malachite green from aqueous solution using low-cost chlorella-based biomass. J Hazard Mater 175:844–849
52. Baek MH, Ijagbemi CO, Se-Jin O, Kim DS (2010) Removal of Malachite Green from aqueous solution using degreased coffee bean. J Hazard Mater 176:820–828
53. Russo ME, Di Natale F, Prigione V, Tigini V, Marzocchella A, Varese GC (2010) Adsorption of acid dyes on fungal biomass: equilibrium and kinetics characterization. Chem Eng J 162:537–545
54. Saha P, Chowdhury S, Gupta S, Kumar I (2010) Insight into adsorption equilibrium, kinetics and thermodynamics of Malachite Green onto clayey soil of Indian origin. Chem Eng J 165:874–882
55. Sarı A, Cıtak D, Tuzen M (2010) Equilibrium, thermodynamic and kinetic studies on adsorption of Sb(III) from aqueous solution using low-cost natural diatomite. Chem Eng J 162:521–527
56. Chowdhury S, Saha P (2010) Sea shell powder as a new adsorbent to remove Basic Green 4 (Malachite Green) from aqueous solutions: equilibrium, kinetic and thermodynamic studies. Chem Eng J 164:168–177
57. Chen Y, Hu J, Wang J (2012) Kinetics and thermodynamics of Cu (II) biosorption on to a novel magnetic chitosan composite bead. Environ Technol 33:2345–2351
58. Finocchio E, Lodi A, Solisio C, Converti A (2010) Chromium (VI) removal by methylated biomass of Spirulina platensis: the effect of methylation process. Chem Eng J 156:264–269
59. Mungapati VS, Yarramuthi V, Nadavala SK, Alla SR, Abburi K (2010) Biosorption of Cu(II), Cd(II) and Pb(II) by Acacia leucocephala bark powder: kinetics, equilibrium, and thermodynamics. Chem Eng J 157:357–365
60. Hutson ND, Yang RT (1997) Theoretical basis for the Dubinin-Radushkevitch (D-R) adsorption isotherm equation. Adsorption 3:189–195
61. Chowdhury S, Mishra R, Saha P, Kushwaha P (2010) Adsorption thermodynamics, kinetics and isosteric heat of adsorption of malachite green onto chemically modified rice husk. Desalination 265:159–168